scientific reports

Check for updates

OPEN

Growth of complex oxide single crystals with high melting point over 2200 °C using tungsten crucible

Yuui Yokota[1,2]✉, Takahiro Suda[1], Takahiko Horiai[2] & Akira Yoshikawa[1,2]

Complex oxide single crystals with melting points (MPs) above 2200 °C cannot be grown from the melt using iridium (Ir) or platinum (Pt) crucibles due to the MP limitations of these materials. To overcome this, we focused on the tungsten (W) crucibles, with MP above 3400 °C. The micro-pulling-down (μ-PD) method employing the W crucible and deoxygenated insulators enabled the growth of oxide single crystals with MP exceeding 2200 °C without any inclusions or deterioration of the W crucible. $La_2Zr_2O_7$ (MP: 2283 °C) and $La_2Hf_2O_7$ (MP: 2418 °C) single crystals with a pyrochlore structure were successfully grown using W crucibles, and they exhibited high transparency after annealing in air. Additionally, we achieved the growth of Lu_3TaO_7 (MP: 2380 °C) single crystals with a density of 9.68 g/cm^3. Lu_3TaO_7 single crystal is a promising scintillator material for high-energy radiation detection due to its ultra-high density and potential for fast decay via Cherenkov light emission. The luminescence and scintillation properties of dopant ions can be clarified in single crystals with rare-earth (RE) ions. These results demonstrate that the advanced growth method is useful tool for the development and study of high-MP optical materials and scintillators.

Keywords High melting point, Tungsten crucible, Crystal growth, Oxide single crystal

Functional oxide bulk single crystals have been developed for various applications such as optical devices, radiation detectors, and piezoelectric sensors. Scintillator single crystals for radiation detectors have been widely studied, with numerous reports on high-melting-point (MP) oxides such as $Lu_3Al_5O_{12}$ [MP: 2020 °C] and Lu_2SiO_5 [MP: 2047 °C] (Fig. 1)[1,2]. The high density and effective atomic number, Z_{eff}, of scintillator single crystals are major advantages of scintillators for high-energy radiation, and many oxide scintillator single crystals with high density and Z_{eff} have been developed worldwide. Most oxide materials containing heavy elements such as rare-earths (*RE*), W, and Ta tend to have MP above 2000 °C.

Various oxide single crystals have been grown from melts by melt-growth methods, such as the Czochralski (Cz), Bridgman–Stockbarger (BS), and Floating Zone (FZ) methods[3–8]. The micro-pulling-down (μ-PD) method is also a melt-growth method, and various functional single crystals have been developed using this method because it has a higher growth rate than other melt-growth methods, including the Cz and BS methods[9–12]. The μ-PD method uses a crucible with a hole at the bottom for the retention of the melt and the formation of the solid–liquid interface. Noble crucibles such as iridium (Ir) and platinum (Pt) crucibles have been generally used because of their chemical stabilities at high temperatures. Although Ir crucible cannot be used in oxygen atmosphere, it has been widely used for crystal growth of oxide single crystals such as garnet, perovskite and pyrochlore-type materials, both commercially and in research. Pt crucible can be used in oxygen atmosphere and is particularly effective for highly volatile oxides. However, the MP of Ir and Pt are 2446 and 1768 °C, respectively, which limits their use for growing high-MP materials such as $RE_2Zr_2O_7$, $RE_2Hf_2O_7$, and RE_3TaO_7. Considering the softening points of Ir and Pt, the maximum practical MP for materials grown by an Ir crucible is approximately 2100 °C (Fig. 1).

Sesquioxide-type single crystals such as Sc_2O_3, Y_2O_3, and RE_2O_3 have been grown using the μ-PD method with a rhenium (Re) crucible[13,14]. However, due to its rarity, poor workability, and high reactivity, Re is rarely used as a crucible material for crystal growth. On the other hand, tungsten (W, MP: 3420 °C) and molybdenum (Mo, MP: 2620 °C) crucibles with higher MPs than Ir and Pt have been used for crystal growth of sapphire single

[1]Institute for Materials Research, Tohoku University, 2-1-1, Katahira, Aoba-ku, Sendai, Miyagi 980-8577, Japan. [2]New Industry Creation Hatchery Center (NICHe), Tohoku University, 6-6-10, Aoba, Aramaki, Aoba-ku, Sendai, Miyagi 980-8579, Japan. ✉email: yui.yokota.a5@tohoku.ac.jp

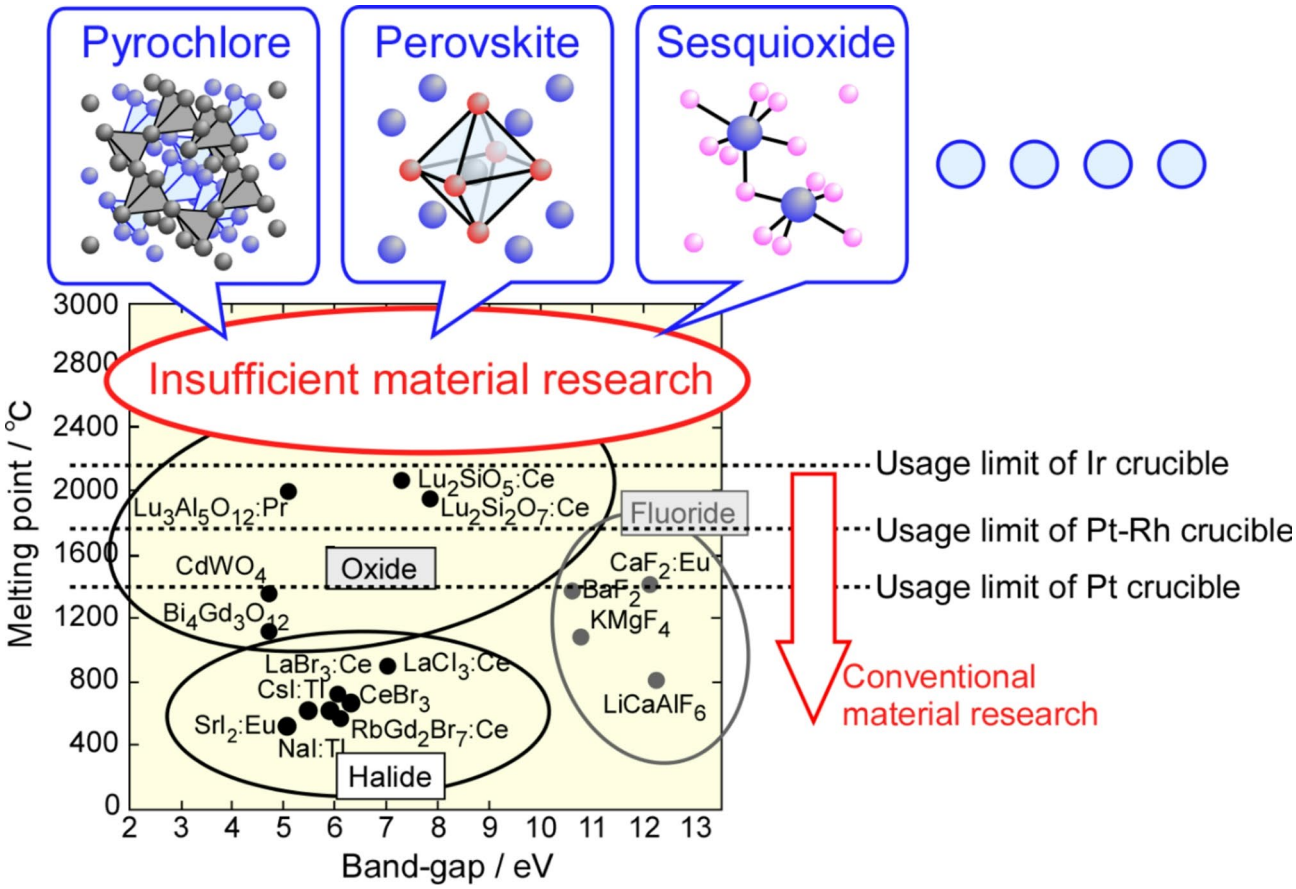

Fig. 1. Relationship between band-gap and MP for oxide, fluoride, and halide scintillator single crystals with usage limit of crucibles.

crystals[15,16]. Bulk sapphire single crystals were grown by the Cz and BS methods[17,18], and shaped sapphire single crystals were grown by the edge-defined film-fed (EFG) and μ-PD methods using specially designed crucibles and dies[15,19].

Recently, oxide single crystals with garnet and perovskite structures have been grown using W and Mo crucibles[20–22]. For oxide single crystals that can be grown in reduction atmosphere, Mo crucible has sometimes been used because of the low cost and good workability. However, Y_2SiO_5 crystals grown in a W crucible exhibited W dendritic branches originating from the crucible[20]. In addition, there are few reports of crystal growth using W and Mo crucibles for complex oxide materials with high MP over 2200 °C, which cannot be grown using the Ir and Pt crucibles.

In this study, we demonstrated the possibility of growing oxide single crystals with MP above 2100 °C using the μ-PD method with W and Mo crucibles. First, we established the growth conditions for single crystal at more than 2200 °C using a $La_2Zr_2O_7$ (LZO) with the MP of 2283 °C in the $RE_2Zr_2O_7$ series[22–24]. Second, $La_2Hf_2O_7$ (LHO) with an MP of 2418 °C in the $RE_2Hf_2O_7$ series[25–27] was grown under the same conditions to evaluate the potential for growing complex oxides above 2400 °C. LZO and LHO have the pyrochlore structure, which is the same crystal structure as Ce-doped $(La, Gd)_2Si_2O_7$ scintillator single crystals with a large light yield and high energy resolution under gamma-ray irradiation[29]. They have attracted attention as gamma-ray scintillators owing to their higher density and effective atomic number compared to La-GPS (Table 1). Additionally, we successfully grew Lu_3TaO_7 (LTO) single crystals with an MP of 2380 °C[30,31], marking the first such achievement globally.

Experimental

The starting materials, La_2O_3, Lu_2O_3, ZrO_2 (>4 N purity), HfO_2, and Ta_2O_5 (>3 N purity) powders were mixed with nominal compositions of $La_2Zr_2O_7$, $La_2Hf_2O_7$, and Lu_3TaO_7 for the growth of undoped single crystals. La_2O_3 powder was dried at 1100 °C for 12 h before weighing to prevent composition deviations caused by high moisture adsorption. The mixed powders were sintered at 1600–1800 °C for 24 h in air using an electric furnace to create $La_2Zr_2O_7$, $La_2Hf_2O_7$, and Lu_3TaO_7. The sintered powders of $La_2Zr_2O_7$, $La_2Hf_2O_7$, and Lu_3TaO_7 with a single phase were placed in a crucible after phase identification using powder X-ray diffraction (XRD). A Φ3 mm die was located at the bottom of the crucible, with a central Φ0.5–0.8 mm capillary connecting the interior to the bottom.

	Z_{eff}	Density [g/cm^3]	m.*p*. [°C]
$La_2Zr_2O_7$	49	5.88	2283
$La_2Hf_2O_7$	64	7.86	2418
Lu_3TaO_7	69	9.68	2380
$PbWO_4$	76	8.28	1123
Lu_2SiO_5	66	7.32	2047
Gd_2SiO_5	59	6.61	1950
$Bi_4Ge_3O_{12}$	75	7.13	1050
$Gd_3Ga_3Al_2O_{12}$	54	6.63	1850

Table 1. Effective atomic number Z_{eff}, density and melting point of LZO, LHO, and LTO with present scintillator single crystals.

Figure 2a shows a schematic diagram of the crystal growth by the μ-PD method for high-MP oxide single crystals using Mo or W crucibles. As a first step, LZO single crystals were grown using the μ-PD method with Mo and W crucibles in an Ar + 3%H_2 atmosphere, which is the same growth condition as the sapphire single crystals using Mo and W crucibles[15,32] to select the suitable crucible and clarify the problems with the growth conditions. The H_2 in the gas mixture created a reducing atmosphere during crystal growth, preventing oxidation of the Mo and W crucibles. The actual furnace has a vacuum chamber [Fig. 2b], and the chamber was purged thrice using a rotary pump to eliminate residual oxygen. The crucible was surrounded by commercial porous ZrO_2 insulators (standard ZrO_2) as the hot zone in a chamber-type μ-PD furnace[12,32], and they were placed in the center of a high-frequency (HF) induction coil. After vacuuming the chamber using a rotary pump and introducing Ar + 3%H_2 mixed gas, the crucible was heated by the HF induction coil directly up to the MP of the LZO. A Φ3 mm W rod was used as the seed, which was connected to *Z*-axis of the furnace and placed just below the crucible. Once the melt appeared at the bottom of the die through the capillary and contacted the W seed, crystal growth was initiated at a growth rate of 0.01–0.10 mm/min by pulling-down the W rod. The solid–liquid interface was monitored during the crystal growth using a charge-coupled device (CCD) camera through opening in the after-heater and insulators.

Next, undoped LZO, LHO, and LTO single crystals were grown under improved conditions using a W crucible and deoxygenated ZrO_2 insulators in an Ar atmosphere. Deoxygenated ZrO_2 insulators played a critical role in the improved growth conditions. They were prepared by heating standard ZrO_2 insulators at 2000 °C for 5–10 h in an Ar atmosphere using a carbon electrical furnace to remove desorbed oxygen from both the surface and interior.

The as-grown crystals were cut and polished to observe their microstructures, chemical compositions, crystallinity, and optical and scintillation properties. In addition, some as-grown crystals were annealed at 1000 °C for 12 h in air to investigate effects of the post-annealing on optical and scintillation properties. Subsequently, doped LZO, LHO, and LTO single crystals were grown via the μ-PD method using a W crucible under improved growth conditions. The selected dopant ions were Ce^{3+}, Eu^{3+}, and Er^{3+}, which can exhibit emissions originating from the 5d–4f and 4f–4f transitions in the visible and infrared wavelength regions and have been used as dopants in existing scintillator single crystals[34–36]. The dopant concentration was fixed at 1 at% relative to the La and Lu sites in LZO, LHO, and LTO, respectively. Mixed powders of *RE*-doped LZO, LHO, and LTO with nominal compositions of $(La_{0.99}RE_{0.01})_2Zr_2O_7$, $(La_{0.99}RE_{0.01})_2Hf_2O_7$, and $(Lu_{0.99}RE_{0.01})_3TaO_7$, respectively, were prepared using starting materials, CeO_2, Eu_2O_3, and Er_2O_3 powders (> 3 N purity) in addition to the starting host materials. The growth of *RE*-doped LZO, LHO, and LTO single crystals was performed under improved growth conditions after sintering under the same conditions as those of undoped LZO, LHO, and LTO. *RE*-doped single crystals were also annealed in air, then cut and polished for subsequent evaluations.

The phases and impurities of the grown crystals were identified by powder XRD using an X-ray diffractometer (D8 DISCOVER, Bruker) after grinding the crystals with an agate mortar. Polished specimens were examined for microstructure using a scanning electron microscope (SEM) with backscattered electron (BSE) (S-3400 N, Hitachi High-Technologies). The chemical composition of each phase in the BSE images of the polished specimens was analyzed using energy-dispersive X-ray spectroscopy (EDX) (E-Max, HORIBA). The crystallinities of the grown crystals were evaluated using Laue images and X-ray rocking curves (XRCs). A Laue image of the polished surface of the grown crystal was obtained using a backscattering Laue camera (RASCO-BL II, RIGAKU). XRC was performed using an in-plane X-ray diffractometer with a Ge (2 2 0) four-crystal monochromator (ATX-E, RIGAKU). The transmittance spectra of the 1-mm-thick polished specimens were measured before and after the post-annealing using an ultraviolet-visible spectrophotometer (V-550, JASCO). Photoluminescence (PL) spectra of the polished specimens in the visible and infrared wavelength ranges were recorded using a spectrofluorometer (FLS920, Edinburgh Instruments) and a fluorescence spectrometer (SS-25, JASCO Corporation), respectively. The X-ray radioluminescence (XRL) spectra of the polished specimens were obtained using a CCD camera (DU420-OE, ANDOR) with an X-ray tube (RASCO-TU, Rigaku) at 40 kV and 25 mA.

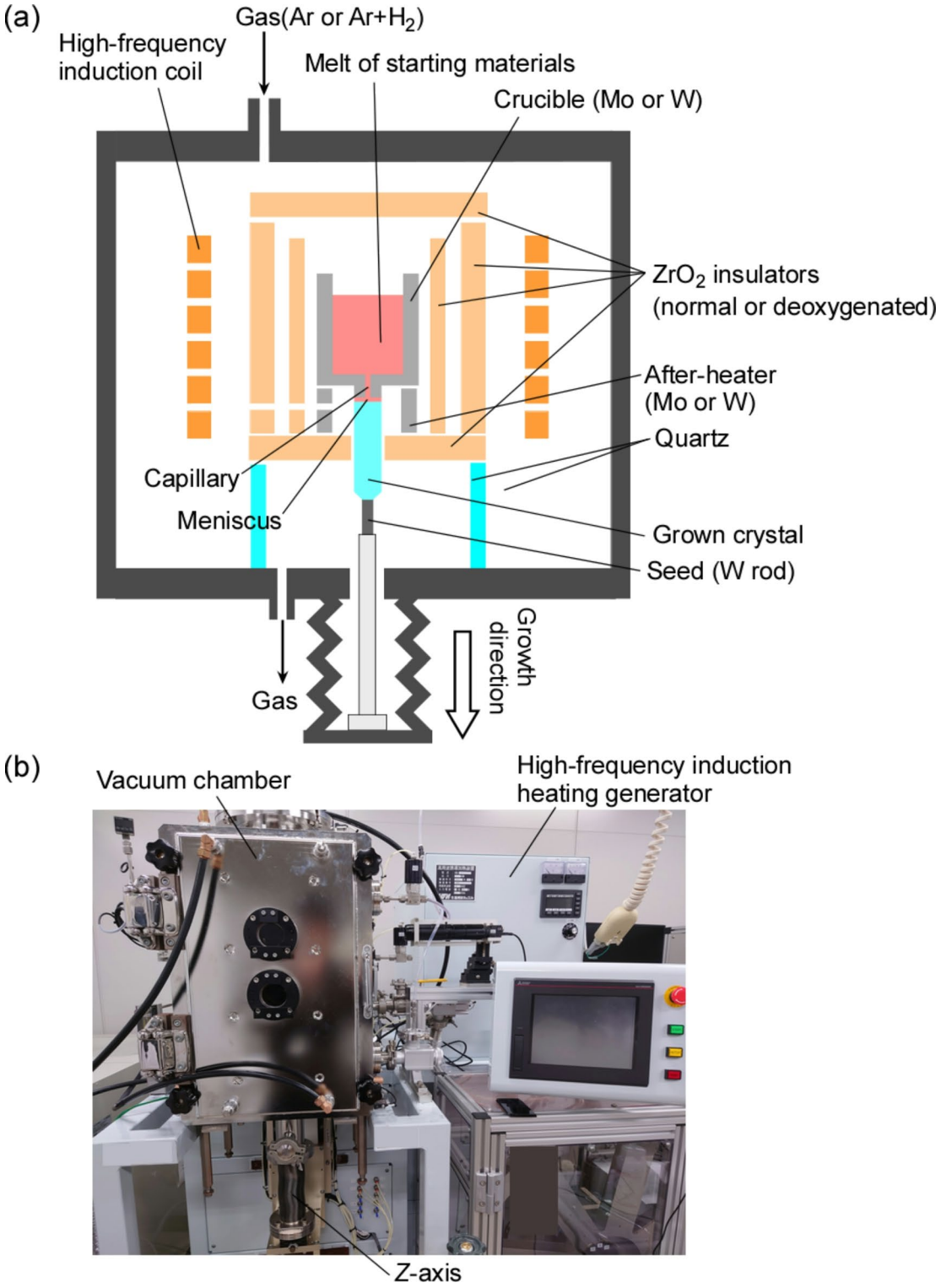

Fig. 2. (**a**) Schematic diagram and (**b**) actual furnace of advanced μ-PD method for crystal growth at high-MP oxides.

Results and discussion

Crystal growth of $La_2Zr_2O_7$ single crystal

First crystal growths of LZO with MP over 2200 °C were performed by the μ-PD method using Mo and W crucibles under Ar + 2%H_2 mixed gas (reduction atmosphere)[37]. In the first crystal growth, commercial porous ZrO_2 tubes and plates were used without any post-processing, and they are standard insulators for μ-PD and Cz methods for oxide single crystals. The solid–liquid interfaces during crystal growth using the Mo and W

crucibles observed by the CCD camera are shown in Fig. 3a,b, respectively. The LZO sintered powder in the crucibles was melted by heating up to the MP of LZO, and the melt spread to the bottom of the die through a capillary. LZO fiber crystals with diameters of approximately Φ3 mm were grown by pulling the melt down using a W rod. Although black fiber crystals were obtained by crystal growth using the Mo crucible, a mottled metallic luster was confirmed on the surface of the as-grown LZO crystal using the Mo crucible and standard insulators under an Ar + 2%H_2 mixed gas [LZO(Mo, Standard)], as shown in Fig. 3a. In addition, the Mo crucible after the crystal growth was clearly deteriorated, and deposits were observed on the top of the crucible, suggesting that the Mo crucible volatilized during the crystal growth in the temperature over 2200 °C and Mo metal re-deposited at the top of the Mo crucible during the crystal growth or cooling process. As a result, it indicated that the repeated use of Mo crucible is difficult in the temperature range over 2200 °C due to the MP of Mo close to the growth temperature. However, there was no clear deterioration of the W crucible after crystal growth, unlike in the Mo crucible [Fig. 3b]. The W crucible has a much higher MP than the Mo crucible and does not react with the melt even at temperature over 2200 °C. However, the as-grown LZO crystal using a W crucible and standard insulators under an Ar + 2%H_2 mixed gas [LZO(W, Standard)] also exhibited a mottled metallic luster on the surface.

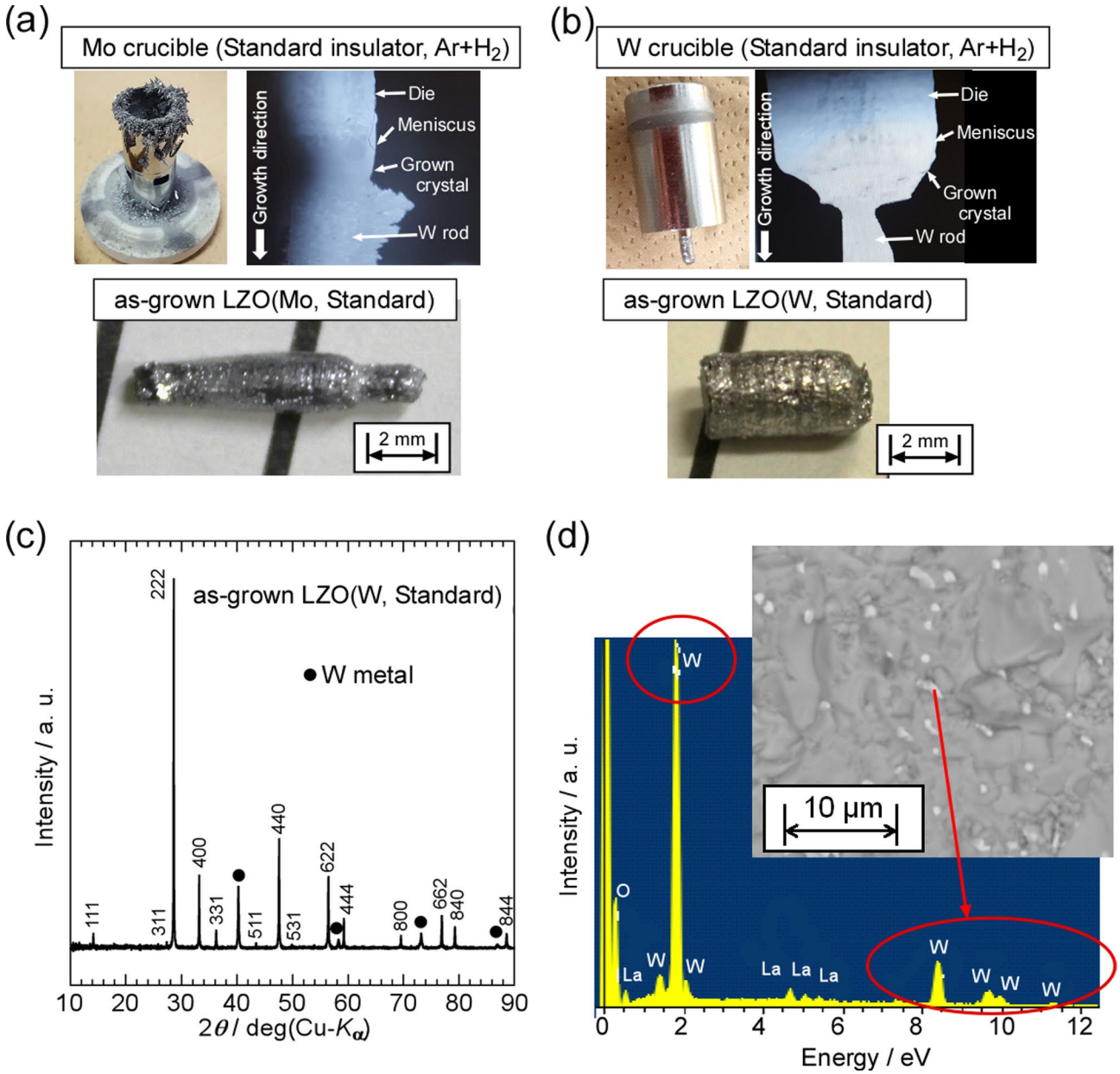

Fig. 3. Solid–liquid interfaces during crystal growth, crucibles after crystal growth and as-grown LZO crystals using (**a**) Mo and (**b**) W crucibles. (**c**) Powder XRD pattern and (**d**) EDX spectrum and BSE image of as-grown LZO (W, Standard) crystal.

Figure 3c shows the powder XRD pattern of the as-grown LZO (W, Standard) crystal. The results indicated that the crystal was composed of the LZO main phase (cubic, Fd $\bar{3}$m) with an impurity phase of W metal. The as-grown LZO (Mo, Standard) also included the impurity phase of Mo metal, in addition to the LZO main phase. In the BSE images of the polished surfaces of both the LZO crystals, impurity particles smaller than 1 mm were observed [Fig. 3d]. The EDX spectra revealed that the impurity particles in the LZO (Mo, Standard) and LZO (W, Standard) crystals were Mo and W, respectively. These results suggest that impurity metals from the crucibles were incorporated into the grown crystals under growth conditions using normal insulators and an Ar + 2% H_2 atmosphere.

Based on the results of the first attempt, LZO crystals were grown by the μ-PD method using the W crucible with deoxygenated ZrO_2 insulators under an Ar atmosphere in the second attempt[37]. Deoxygenated ZrO_2 insulators were prepared by annealing the normal ZrO_2 insulator under Ar atmosphere at 2000 °C in the carbon furnace to remove oxygen from the insulator at high temperature [Fig. 4a]. The suppression of oxygen release from the ZrO_2 insulator at high temperatures during crystal growth is expected due to the deoxygenation process. In the improved growth conditions compared to the first attempt, a deoxygenated ZrO_2 insulator was used instead of the standard ZrO_2 insulator to prevent the W crucible from being oxidized by oxygen from the insulators. Because of the deoxygenated insulators, the W crucible could be used during the crystal growth and did not show any deterioration, even in an Ar atmosphere. The solid–liquid interface was stable during crystal growth from the initial to the final stages, and an as-grown LZO fiber crystal with a constant diameter was obtained [LZO (W, Deoxygenated)], as shown in Fig. 4b. The as-grown LZO (W, Deoxygenated) crystal had no mottled metallic luster on its surface, unlike the as-grown LZO (W, Standard) crystal.

Compared with the LZO (W, Standard) crystal, the diffraction peaks from the W particles disappeared in the powder XRD pattern of the LZO (W, Deoxygenated) crystal, indicating that the crystal was a single phase of LZO without any impurity phases [Fig. 4c]. In addition, no W particles were detected in the BSE image of the polished LZO (W, Deoxygenated) crystal, unlike that of the LZO (W, Standard) crystal. Figure 4d shows the XRC pattern of the (2 2 2) diffraction peak for the polished LZO (W, Deoxygenated) specimen, which indicates a sharp and symmetric peak without satellite peaks or shoulders. The full width at half maximum (FWHM) of the XRC was 150 arcsec (0.0418°), indicating crystallinity comparable to that of single crystals grown using the μ-PD method[15,32]. A clear Laue pattern was also observed in the Laue image of the polished specimen. These results revealed that the improved growth condition could suppress the inclusion come from the W crucible and grow single crystals without any impurities under high temperature over 2200 °C. In other words, the deoxygenated ZrO_2 insulators did not release oxygen at high temperatures. As a result, the W crucible was not oxidized during crystal growth.

The polished specimen prepared from the as-grown LZO crystal showed almost no transparency and was black in color. The effect of annealing on the polished specimens of LZO (W, Standard) and LZO (W, Deoxygenated) crystals was investigated to clarify the cause of the black color. The polished LZO (W, Standard) and LZO (W, Deoxygenated) specimens before and after annealing at 1000 °C in air are shown in Fig. 4e. After annealing, the LZO (W, Standard) specimen, including the W metal impurity, crumbled and became a white powder, suggesting that the collapse of the specimen was due to the expansion of W metal in the LZO phase by oxidation of W metal at high temperature in air during annealing. In contrast, the LZO (W, Deoxygenated) crystals became colorless and transparent without collapsing or cracking upon annealing in air. Figure 4f shows the transmittance spectra of the LZO (W, Deoxygenated) specimens before and after annealing. The transmittance of the polished LZO (W, Deoxygenated) specimen, which was almost non-transparent, was dramatically improved by the annealing, reaching over 70% in the wavelength range of 400–800 nm. These annealing results demonstrate that the as-grown LZO (W, Deoxygenated) crystal included oxygen defects generated during crystal growth, which could be compensated for by annealing in air. In the previous paper about the mechanism of oxygen defect formation and healing in $TiO_{2-\delta}$ single crystal by annealing[38], the dark $TiO_{2-\delta}$ contains oxygen defects which forms absorption band in the band-gap, and annealing in oxygen atmosphere compensates oxygen defects, resulting in colorless TiO_2 with almost stoichiometric composition. Therefore, it is suggested that absorption caused by oxygen defects in the as-grown LZO (W, Deoxygenated) crystal almost completely disappeared by post-annealing in air and it became the colorless and transparent crystal. In addition, the post-annealed transparent specimen maintained high transparency even after one year under ambient storage.

Crystal growth of $La_2Hf_2O_7$ and Lu_3TaO_7 single crystals

Next, LHO and LTO crystals with the MP around 2400 °C were grown using the W crucible and deoxygenated ZrO_2 insulators in Ar atmosphere[39]. The solid–liquid interfaces during the crystal growth of the LHO and LTO crystals were also stable, whereas the melt overflowed at the end of the crystal growth for the LHO crystal, causing an increase in the crystal diameter. Under the same improved growth conditions, LHO and LTO crystals could be grown without W inclusion and deterioration of W crucible even over 2400 °C. Figure 5a shows the as-grown LHO and LTO crystals grown under the improved growth conditions [LHO (W, Deoxygenated) and LTO (W, Deoxygenated)] and the polished specimens after annealing in air. There was no mottled metallic luster for either the as-grown LHO or LTO crystals, and the polished specimens of the LHO and LTO crystals after annealing in air exhibited high transparency without collapse. All diffraction peaks in the powder XRD patterns of LHO and LTO crystals could be identified by the phases of LHO and LTO, respectively [Fig. 5b], indicating that the improved growth condition was effective in preventing contamination of the W metal for crystal growth even over 2400 °C. The XRCs of the polished LHO and LTO specimens showed symmetric peaks without satellite peaks and shoulders, and clear Laue images were obtained [Fig. 5c]. The results revealed that the oxide single crystal with higher melting point than 2400 °C can be grown by the μ-PD method using W crucible and deoxygenated insulators without the degradation of the crucible and inclusions in the grown crystal.

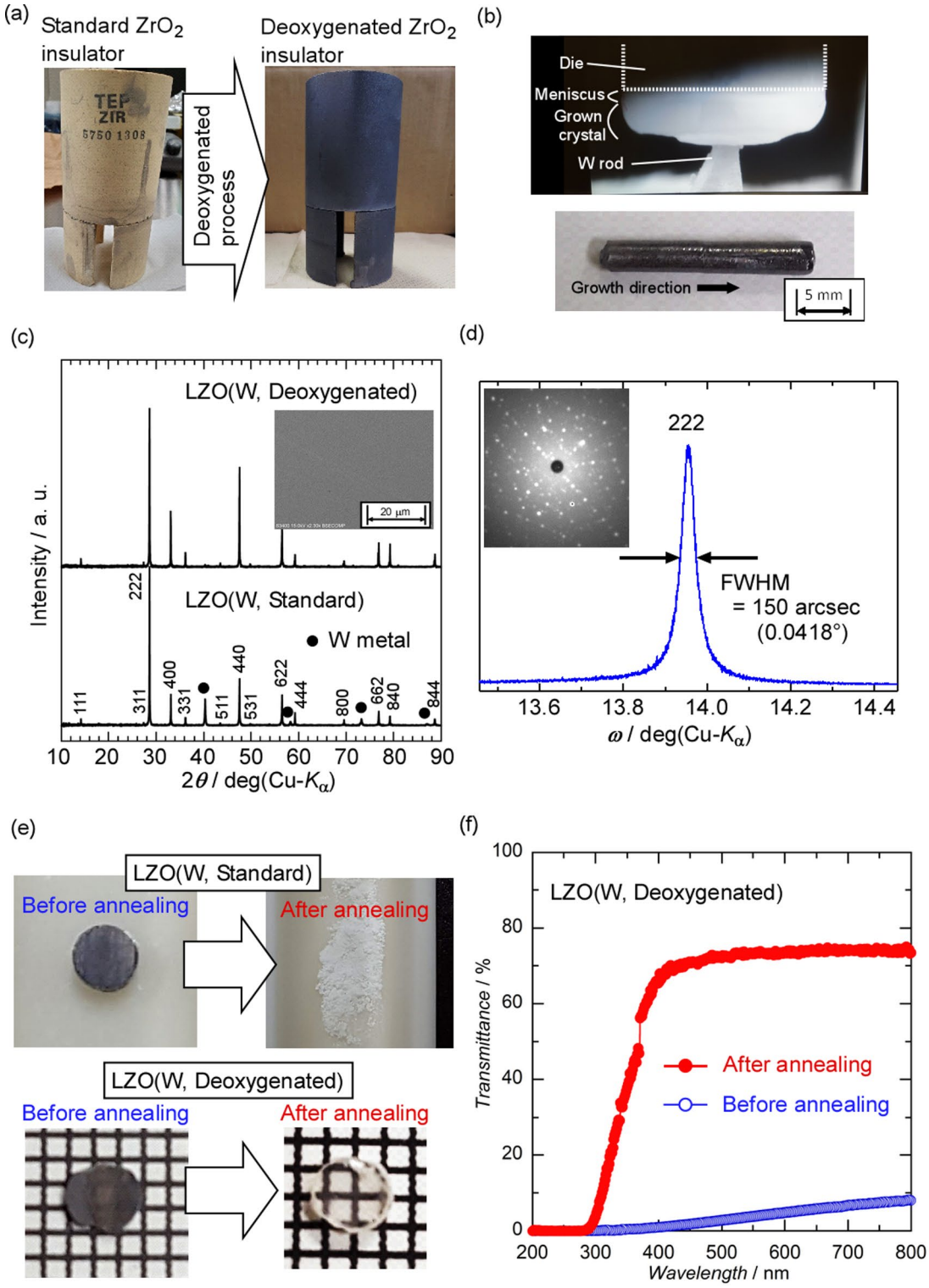

Fig. 4. (**a**) Standard and deoxygenated ZrO_2 insulators. (**b**) Solid–liquid interface during the crystal growth of LZO using W crucible and deoxygenated insulator and as-grown LZO (W, Deoxygenated) crystal. (**c**) Powder XRD patterns of LZO (W, Standard) and LZO (W, Deoxygenated) crystals. Inset is BSE image of polished LZO (W, Deoxygenated) specimen. (**d**) XRC and Laue image of the LZO (W, Deoxygenated) crystal. (**e**) Polished LZO (W, Standard) and LZO (W, Deoxygenated) specimens before and after annealing. (**f**) Transmittance spectra of polished LZO (W, Deoxygenated) specimens before and after annealing.

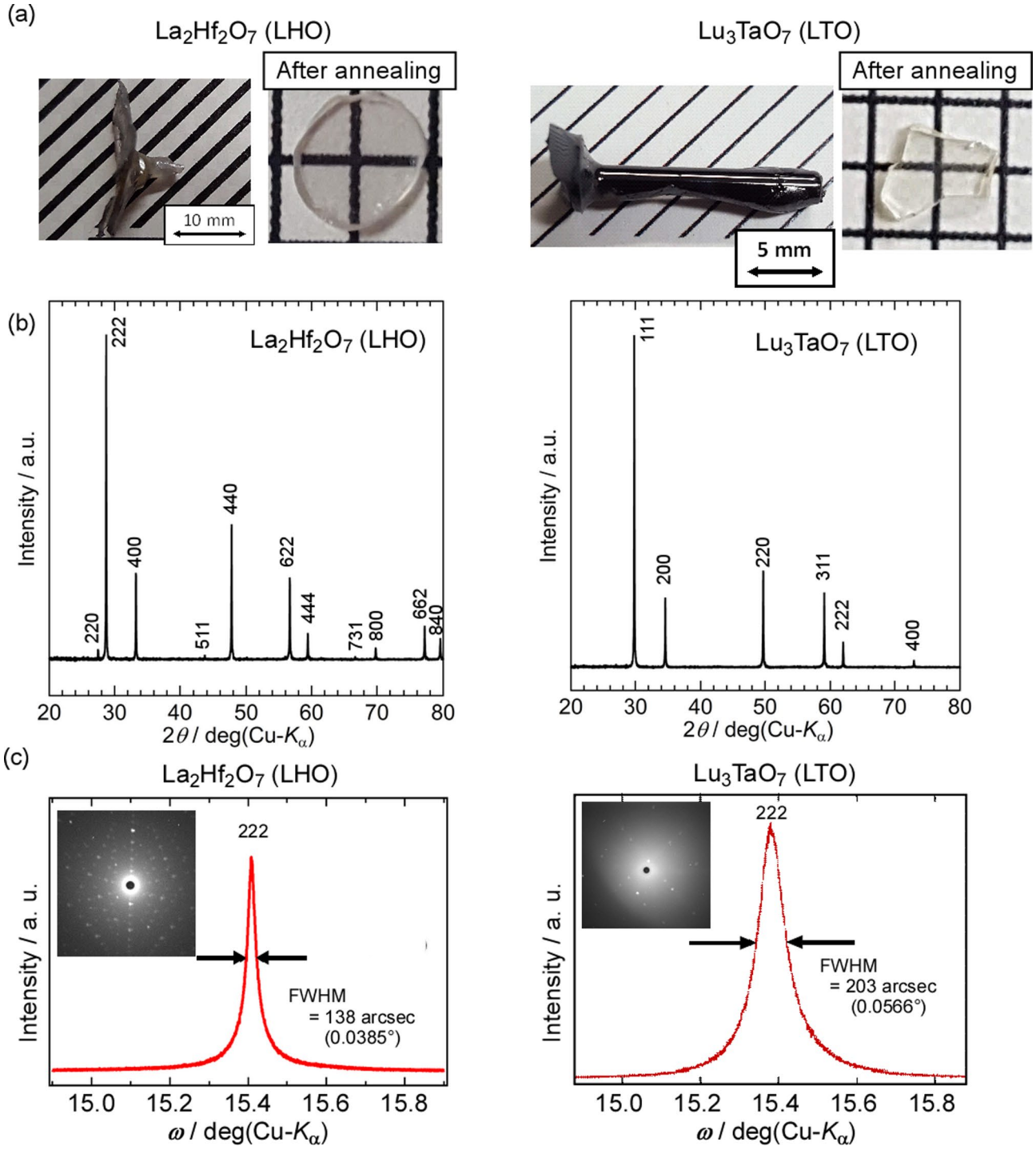

Fig. 5. (**a**) As-grown and annealed LHO and LTO single crystals grown using W crucible and deoxygenated insulator. (**b**) Powder XRD patterns and (**c**) XRCs and Laue images of LHO and LTO single crystals.

Crystal growth and optical and scintillation properties of *RE*-doped LZO, LHO, and LTO single crystals

To investigate the effectiveness of the improved growth conditions for the growth of high-MP oxide single crystals with dopant ions, Eu-doped LZO [Eu: LZO], Eu-doped LHO [Eu: LHO], Er-doped LHO [Er: LHO], and Ce-doped LTO [Ce: LTO] single crystals were grown using the W crucible and deoxygenated ZrO_2 insulators in an Ar atmosphere[40]. All the LZO, LHO, and LTO crystals with each dopant ion were obtained from melt-like undoped crystals. The as-grown *RE*-doped LZO, LHO, and LTO crystals and the polished specimens are shown in Fig. 6a. All polished specimens showed high transparency after annealing, except for the Er: LHO crystal. Figure 6b is powder XRD patterns of the as-grown *RE*-doped LZO, LHO, and LTO crystals, and they indicated

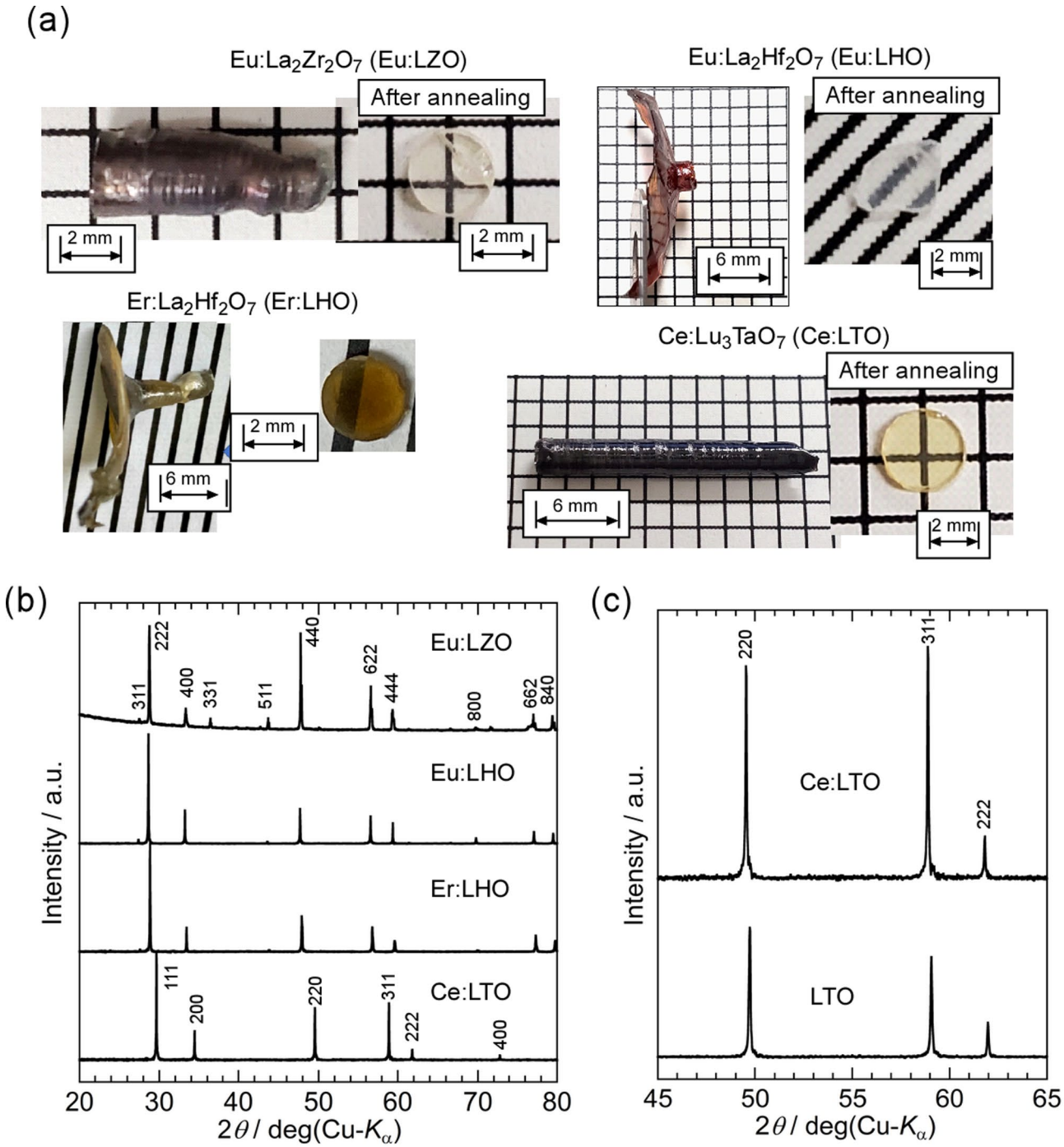

Fig. 6. (**a**) As-grown and annealed Eu: LZO, Eu: LHO, Er: LHO, and Ce: LTO single crystals. (**b**) Powder XRD patterns of Eu: LZO, Eu: LHO, Er: LHO, and Ce: LTO single crystals. (**c**) Powder XRD patterns of LTO and Ce: LTO single crystals.

that all grown crystals were in a single phase of the target materials, LZO, LHO, and LTO. In the powder XRD patterns of LTO and Ce: LTO single crystals [Fig. 6c], diffraction peaks shifted to smaller values of 2θ and the lattice parameter increased by the Ce-doping, suggesting that Lu^{3+} ion in LTO was replaced by Ce^{3+} ion with larger ionic radius.

In the PL and XRL spectra of the polished Eu: LZO and Eu: LHO specimens [Fig. 7a], sharp emission peaks originating from the 4f–4f transition of the Eu^{3+} ion appeared at approximately 600 nm. A large broad absorption peak of Eu^{3+} ions at approximately 300 nm was observed in the excitation spectra of the Eu: LZO and Eu: LHO specimens. The emission and absorption peaks in the PL spectra were similar to those of conventional optical and scintillation materials containing Eu^{3+} dopant ions[41,42]. In addition, the Er: LHO single crystals showed emission peaks originating from the Er^{3+} ions at approximately 550 nm in the visible wavelength region and at

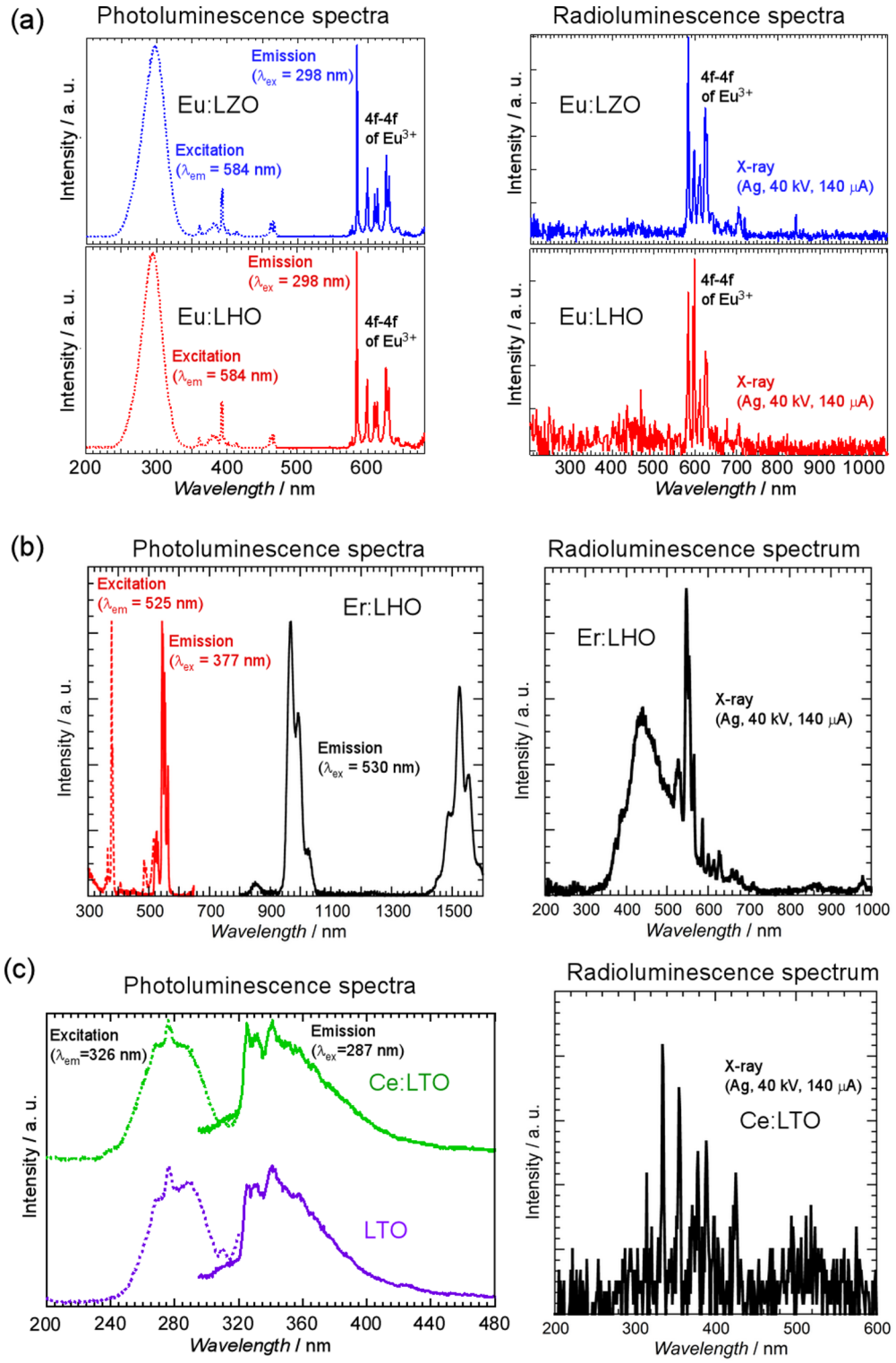

Fig. 7. (**a**) PL and XRL spectra of Eu: LZO and Eu: LHO single crystals. (**b**) PL and XRL spectra of Er: LHO single crystal. (**c**) PL spectra of undoped LTO and Ce: LTO single crystals and XRL spectrum of Ce: LTO single crystal.

approximately 1000 and 1550 nm in the infrared wavelength region as shown in Fig. 7b[40]. Emission peaks in the visible and infrared wavelength regions were also observed in the XRL spectrum.

Figure 7c shows the excitation and emission spectra of polished LTO and Ce: LTO specimens under 326 and 287 nm excitation, respectively. A broad emission peak at approximately 330 nm was observed in the emission spectra of both LTO and Ce: LTO single crystals. The emission was also observed in the XRL spectrum of Ce:

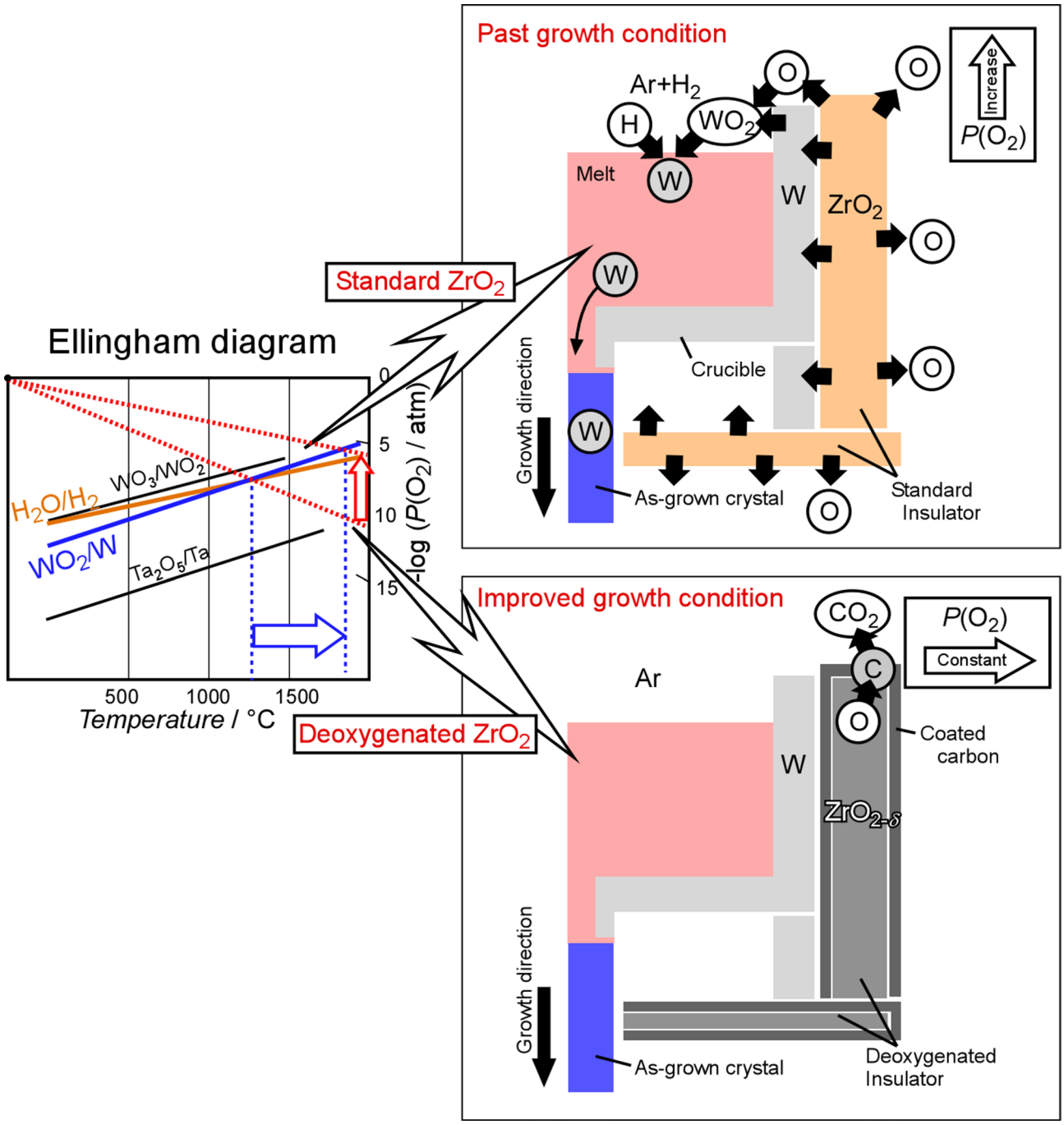

Fig. 8. Ellingham diagram and growth mechanisms in the crystal growths of LZO (W, Standard) and LZO (W, Deoxygenated) crystals by μ-PD method using W crucible.

LTO single crystal. However, there was no emission peak originating from the Ce^{3+} ion in the emission spectrum of the Ce: LTO single crystal, suggesting that the emission peak at approximately 330 nm was attributable to the LTO host material, such as the self-trapped exciton (STE). In the previous report about the LTO ceramics[43], band-gap of the LTO was estimated using the absorption spectrum and it is approximately 4.7 eV. However, most of the exisitng Ce-doped oxide scintillators have band-gaps from 5 to 10 eV[44]. Therefore, it is suggested that band-gap of the LTO is too small to obtain emission from 5d-4f transition of Ce^{3+} ion. These results demonstrate that single crystals of high-MP oxides containing dopant ions can be grown in a W crucible, and their optical and scintillation properties can be efficiently clarified using the advanced growth method.

Discussion of crystal growth using W crucible and deoxygenated insulators

Figure 8 shows the Ellingham diagram and growth mechanism of the crystal growths of LZO (W, Standard) and LZO (W, Deoxygenated) crystals. After three gas replacements using a rotary pump, the estimated oxygen

partial pressure [$P(O_2)$] in the chamber of the μ-PD furnace was less than 10^{-2} Pa. Assuming that the $P(O_2)$ in the chamber remains at this level during crystal growth, W metal is stable above 1220 °C without oxidation, according to the Ellingham diagram. However, the standard ZrO_2 insulator has a property of releasing oxygen in a low $P(O_2)$ atmosphere at high temperature due to the oxygen non-stoichiometry ($ZrO_{2\pm\delta}$). As a result, $P(O_2)$ in the chamber increased, and the temperature range in which tungsten oxide (WO_2) is stable expanded toward higher temperatures. The following reactions can then occur around standard ZrO_2 insulators under an $Ar + H_2$ atmosphere, and W metal is mixed into the melt:

$$ZrO_2 \rightarrow ZrO_{2-\delta} + \frac{\delta}{2}O_2 \uparrow$$

$$W\,(\text{Crucible}) + O_2 \rightarrow WO_2 \uparrow$$

$$WO_2 + 2H_2 \rightarrow W\,(\text{Inclusion}) + 2H_2O$$

In contrast, the deoxygenated ZrO_2 insulator can prevent oxygen release at high temperatures, because the oxygen in the insulator is removed in advance by the deoxygenation process. Even if a small amount of oxygen is released from the deoxygenated ZrO_2 insulator, it is captured by the carbon coated on the surface of the insulator as follows:

$$O_2 + C(\text{Coated on insulator}) \rightarrow CO_2$$

As a result, low $P(O_2)$ in the chamber can be maintained during crystal growth, and W does not react with oxygen under low $P(O_2)$, allowing the W crucible to be used, even at high temperatures. Therefore, oxide single crystals with high MP could be grown without W contamination under improved growth conditions.

Recently, the growth of RE sesquioxide-type single crystals such as Sc_2O_3, Y_2O_3, and Lu_2O_3 has been achieved using W crucibles and deoxygenated ZrO_2 insulators, and material research on solid-solution RE sesquioxide-type single crystals has been progressing[45,46]. In addition, crystal growth has been achieved in RE perovskite-type single crystals, such as $YScO_3$, $GdScO_3$, and their solid solutions, and the scope of exploration of the μ-PD method using a W crucible is gradually expanding.

Conclusions

Advanced crystal growth method using the W crucible and deoxygenated ZrO_2 insulator for oxide single crystals with high MP over 2200 °C has been established for material research of functional single crystals in the high temperature region. Undoped and *RE*-doped LZO, LHO, and LTO single crystals with higher MP than 2200 °C could be grown by the advanced crystal growth method, and their optical and scintillation properties were elucidated. The result of XRC indicates that the defect rate of single crystal grown by the advanced crystal growth method is comparable to that of the standard μ-PD method. In addition, all melt was crystalized in the method, and the yield is almost 100%. The successful results of various crystal growths involving sesquioxide- and perovskite-type systems indicate the possibility of extending single crystals to other material systems that have not been previously explored. Among the single crystals developed in this study, the LTO in the RE_3TaO_7 series has a density larger than that of the $PbWO_3$ scintillator, suggesting that LTO has potential as a gamma-ray scintillator with high stopping power for applications in medical imaging and high-energy physics. In the future, it is expected that advanced crystal growth using the W crucible will expand material research for functional single crystals of high-MP oxide materials with various crystal systems. In addition, W crucible can be reused by acid washing with hydrochloric acid like Ir and Pt crucibles, and the abundance of W in the Earth's crust, approximately 1000 times that of Re and Ir, contributes to the sustainable production of single crystals. Improvement of processing to W has made it possible to obtain hard W crucible, and W crucible has an advantage over Mo crucible in terms of resistance to deformation during crystal growth. The standard μ-PD method can grow single crystal fibers up to approximately 10 mm in diameter and the advanced μ-PD method using W crucible is the same. Crystal growth using W crucible and deoxygenated insulator can be also applied to Cz method, and the advanced Cz method using W crucible has great advantages in terms of cost and productivity for commercial use if the method is established.

Data availability

Data is provided within the manuscript. Raw data were generated at Tohoku University. Derived data supporting the findings of this study are available from the corresponding author, Yuui Yokota, on request.

Received: 7 June 2025; Accepted: 17 July 2025
Published online: 08 August 2025

References

1. Ogino, H. et al. Growth and scintillation properties of Pr-doped $Lu_3Al_5O_{12}$ crystals. *J. Cryst. Growth*. **287**, 335–338 (2006).
2. Melcher, C. L. & Schweitzer, J. S. A promising new scintillator: Cerium-doped lutetium oxyorthosilicate. *Nucl. Instru Meth Phys. Res. A*. **314**, 212–214 (1992).
3. Czochralski, J. Ein neues Verfahren Zur Messung der kristallisationsgeschwindigkeit der Metalle. *Z. Phys. Chem*. **92**, 219–221 (1918).
4. Melcher, C. L., Manente, R. A., Peterson, C. A. & Schweitzer, J. S. Czochralski growth of rare Earth oxyorthosilicate single crystals. *J. Cryst. Growth*. **128**, 1001–1005 (1993).

5. BridgmanP. W. Certain physical properties of single crystals of tungsten, antimony, bismuth, tellurium, cadmium, zinc, and Tin. *Proc. Am. Acad. Arts Sci.* **60**, 305–283 (1925).
6. Yokota, Y., Horiai, T. & Yoshino, M. Inorganic Scintillator and Crystal Growth Methods. *Wiley-VCH* (2024).
7. Kimura, S. & Kitamura, K. Floating zone crystal growth and phase equilibria: A review. *J. Am. Ceram.* **75**, 1440–1446 (1992).
8. Balbashov, A. M. & Egorov, S. K. Apparatus for growth of single crystals of oxide compounds by floating zone melting with radiation heating. *J. Cryst. Growth*. **52**, 498–504 (1981).
9. Yoon, D. H. & Fukuda, T. Characterization of $LiNbO_3$ micro single crystals grown by the micro-pulling-down method. *J. Cryst. Growth*. **144**, 201–206 (1994).
10. Yoshikawa, A. & Chani, V. Growth of optical crystals by the Micro-Pulling-Down method. *MRS Bull.* **34**, 266–270 (2009).
11. Yokota, Y. et al. Development of novel growth methods for halide single crystals. *Opt. Mater.* **65**, 46–51 (2017).
12. Yokota, Y. et al. Crystal growth of Na-Co-Doped Ce:$LiCaAlF_6$ single crystals and their optical, scintillation, and physical properties. *Cryst. Growth Des.* **11**, 4775–4779 (2011).
13. Fukabori, A. et al. Growth of Y_2O_3, Sc_2O_3 and Lu_2O_3 crystals by the micro-pulling-down method and their optical and scintillation characteristics. *J. Cryst. Growth*. **318**, 823–827 (2011).
14. Mun, J. H., Novoselov, A., Yoshikawa, A., Boulon, G. & Fukuda, T. Growth of Yb^{3+}-doped Y_2O_3 single crystal rods by the micro-pulling-down method. *Mater. Res. Bull.* **40**, 1235–1243 (2005).
15. Yokota, Y. et al. Growth and crystallinity of shaped and multiple Sapphire crystals by a micro-pulling-down method. *J. Cryst. Growth*. **318**, 983–986 (2011).
16. Miyagawa, C., Kobayashi, T., Taishi, T. & Hoshikawa, K. Demonstration of crack-free c-axis Sapphire crystal growth using the vertical Bridgman method. *J. Cryst. Growth*. **372**, 95–99 (2013).
17. Nguyen, T. P., Hsieh, Y. T., Chen, J. C., Hu, C. & Nguyen, H. B. Effect of crucible and crystal rotations on the convexity and the thermal stress in large size Sapphire crystals during Czochralski growth. *J. Cryst. Growth*. **468**, 514–525 (2017).
18. Suzuki, T., Shirotsuki, K., Taishi, T. & Hoshikawa, K. Contact angle of Sapphire melt and bubble generation on crucible material. *J. Cryst. Growth* **8**, 508–510 (2024).
19. LaBelle, H. E. Jr. EFG, the invention and application to Sapphire growth. *J. Cryst. Growth*. **50**, 8–17 (1980).
20. Tkachenko, S. et al. Control of optical properties of YAG crystals by thermal annealing. *J. Cryst. Growth*. **483**, 195–199 (2018).
21. Kamada, K. et al. Multiple shaped-crystal growth of oxide scintillators using mo crucible and die by the edge defined film fed growth method. *J. Cryst. Growth*. **535**, 125510 (2020).
22. Yoshino, M., Kotaki, A., Yokota, Y., Horiai, T. & Yoshikawa, A. Shape-Controlled Crystal Growth of $Y_3Al_5O_{12}$: Ce Single Crystals with Application of Micro-Pulling-Down Method and Mo Crucibles, and Their Scintillation Properties. *Crystals* **12**, 1215 (2022).
23. Wang, Z. et al. Transparent $La_{2-x}Gd_xZr_2O_7$ ceramics obtained by combustion method and vacuum sintering. *J. Alloys Compd.* **585**, 497–502 (2014).
24. Zhang, A., Lü, M., Yang, Z., Zhou, G. & Zhou, Y. Systematic research on $RE_2Zr_2O_7$ (RE = La, nd, Eu and Y) nanocrystals: preparation, structure and photoluminescence characterization. *Solid State Sci.* **10**, 74–81 (2008).
25. An, L. Q., Ito, A. & Goto, T. Fabrication of transparent $La_2Zr_2O_7$ by reactive spark plasma sintering. *Key Eng. Mater.* **484**, 135–138 (2011).
26. Gupta, S. K. et al. On comparison of luminescence properties of $La_2Zr_2O_7$ and $La_2Hf_2O_7$ nano-particles. *J. Am. Ceram. Soc.* **103**, 235–248 (2020).
27. Trojan-Piegza, J., Gierlotka, S., Zych, E. & Lojkowski, W. Spectroscopic studies of nanopowder and nanoceramics $La_2Hf_2O_7$:Pr scintillator. *J. Am. Ceram. Soc.* **97**, 1595–1601 (2014).
28. Gupta, S. K. et al. Lanthanides doped lanthanum Hafnate as multicolored phosphors for warm white lighting and scintillators. *Chem. Eng. J.* **379**, 122314 (2020).
29. Suzuki, A. et al. Fast and High-Energy-Resolution oxide scintillator: Ce-Doped (La,Gd)2Si2O7. *Appl. Phys. Express*. **5**, 102601 (2012).
30. Zhang, Y. et al. Luminescence enhancement of Lu_3TaO_7:Eu^{3+}@Lu_3TaO_7 red-emitting nanophosphors. *Eur. J. Inorg. Chem.* **2015**, 690–695 (2015).
31. Xing, X. et al. High-Temperature phase relations in the Lu_2O_3-Ta_2O_5 system. *J. Am. Ceram. Soc.* **99**, 1042–1046 (2016).
32. Yokota, Y., Ohashi, Y. & Yoshikawa, A. Development of a three-dimensional-micro-pulling-down method and growth of spring-shaped Sapphire single crystals. *CrystEngComm* **26**, 5364–5370 (2024).
33. Yokota, Y. et al. Fabrication of metallic fibers with high melting point and poor workability by unidirectional solidification. *Adv. Eng. Mater.* **20**, 1700506 (2018).
34. Yokota, Y. et al. Development of modified micro-pulling-down method for bromide and chloride single crystals. *J. Cryst. Growth*. **318**, 908–911 (2011).
35. Yokota, Y., Kurosawa, S., Nishimoto, K., Kamada, K. & Yoshikawa, A. Growth of Eu:SrI_2 bulk crystals and their scintillation properties. *J. Cryst. Growth*. **401**, 343–346 (2014).
36. Pejchal, J. et al. Luminescence mechanism in Doubly-doped LaF_3:Er,Nd VUV scintillator. *IEEE Trans. Nucl. Sci.* **57**, 1196–1199 (2010).
37. Suda, T. et al. Crystal growth of $La_2Zr_2O_7$ by micro-pulling-down method using mo and W crucibles. *J. Cryst. Growth*. **575**, 126357 (2021).
38. Sekiya, T. et al. Kodaira, defects in anatase TiO_2 single crystal controlled by heat treatments. *J. Phys. Soc. Jpn* **73**(3), 703–710 (2004).
39. Suda, T. et al. Crystal growth of $La_2Hf_2O_7$ by micro-pulling-down method using W crucible. *J. Cryst. Growth*. **583**, 126547 (2022).
40. Hayashi, N. et al. Crystal growth, luminescence, and scintillation properties of Er-doped $La_2Hf_2O_7$ single crystal. *Jpn J. Appl. Phys.* **63**, 03SP15 (2024).
41. Ronda, C. R. Phosphors for lamps and displays: an applicational view. *J. Alloys Compd.* **225**, 534–538 (1995).
42. Mączka, M., Bednarkiewicz, A., Mendoza-Mendoza, E., Fuentes, A. F. & Kępiński, L. Low-temperature synthesis, phonon and luminescence properties of Eu doped $Y_3Al_5O_{12}$ (YAG) nanopowders. *Mater. Chem. Phys.* **143**, 1039–1047 (2014).
43. Sang, W. et al. Thermophysical performances of $(Sm_{1-x}Lu_x)_3TaO_7$ (x = 0, 0.1, 0.3 and 0.5) ceramics. Proce. *Appl. Ceram.* **15[3]**, 306–313 (2021).
44. Dorenbos, P. Light output and energy resolution of Ce^{3+}-doped scintillators. *Nucl. Instr Meth Phys. Res. A*. **486**, 208–213 (2002).
45. Yuka Abe, T. et al. Yuji ohashi, Shunsuke kurosawa, Kei kamada, Martin nikl, Akira yoshikawa, crystal growth and evaluating luminescent properties of Eu-doped (Y, lu, Sc)$_2O_3$ for optical thermometry. *J. Lumin.* **280**, 121118 (2025).
46. Yuka Abe, T. et al. Akira yoshikawa, crystal growth and temperature dependence of luminescence characteristics of Pr^{3+} and Tb^{3+} doped solid-solution sesquioxide single crystals. *J. Mater. Chem. C.* **13**, 8032–8042 (2025).

Acknowledgements

This work was partially supported by the Japan Society for the Promotion of Science (JSPS) KAKENHI, Grant-in-Aid for Scientific Research [JP16H06439] and the Japan Science and Technology Agency (JST) Adaptable & Seamless Technology Transfer Program through Target-driven R&D (A-STEP) [AS272S003a] [JPMJTR232C].

Author contributions

Yuui Yokota wrote the main manuscript text and Takahiro Suda and Takahiko Horiai performed crystal growth and evaluations. All authors reviewed the manuscript.

Declarations

Competing interests

The authors declare no competing interests.

Additional information

Correspondence and requests for materials should be addressed to Y.Y.

Reprints and permissions information is available at www.nature.com/reprints.

Publisher's note Springer Nature remains neutral with regard to jurisdictional claims in published maps and institutional affiliations.